Title: Inhibition of celecoxib crystallization by mesoporous silica - molecular dynamics studies leading to the discovery of the stabilization origin

Author: Daniel Kramarczyk, Justyna Knapik-Kowalczuk, Wojciech Smolka, Maria Ferreira Monteiro, Lidia Tajber, Marian Paluch

Citation style: Kramarczyk Daniel, Knapik-Kowalczuk Justyna, Smolka Wojciech, Monteiro Maria Ferreira, Tajber Lidia, Paluch Marian. (2022). Inhibition of celecoxib crystallization by mesoporous silica - molecular dynamics studies leading to the discovery of the stabilization origin. "European Journal of Pharmaceutical Sciences" (2022), Vol. 0, art. no. 106132, s. 1-27.
DOI: 10.1016/j.ejps.2022.106132

Inhibition of celecoxib crystallization by mesoporous silica – molecular dynamics studies leading to the discovery of the stabilization origin

Daniel Kramarczyk , Justyna Knapik-Kowalczuk , Wojciech Smolka , Maria Ferreira Monteiro , Lidia Tajber , Marian Paluch

PII: S0928-0987(22)00017-3
DOI: https://doi.org/10.1016/j.ejps.2022.106132
Reference: PHASCI 106132

To appear in: *European Journal of Pharmaceutical Sciences*

Received date: 26 October 2021
Revised date: 15 January 2022
Accepted date: 18 January 2022

Please cite this article as: Daniel Kramarczyk , Justyna Knapik-Kowalczuk , Wojciech Smolka , Maria Ferreira Monteiro , Lidia Tajber , Marian Paluch , Inhibition of celecoxib crystallization by mesoporous silica – molecular dynamics studies leading to the discovery of the stabilization origin, *European Journal of Pharmaceutical Sciences* (2022), doi: https://doi.org/10.1016/j.ejps.2022.106132

Inhibition of celecoxib crystallization by mesoporous silica – molecular dynamics studies leading to the discovery of the stabilization origin

Daniel Kramarczyk[1,*] daniel.kramarczyk@smcebi.edu.pl, Conceptualization, Investigation, Methodology, Validation, Visualization, Writing - original draft, Justyna Knapik-Kowalczuk[1,*] justyna.knapik-kowalczuk@us.edu.pl, Conceptualization, Methodology, Supervision, Validation, Writing - review & editing, Wojciech Smolka[2], Investigation, Maria Ferreira Monteiro[3], Investigation, Lidia Tajber[3], Methodology, Writing-review & editing, Marian Paluch[1], Conceptualization, Funding acquisition, Supervision, Writing - review & editing

[1]Faculty of Science and Technology, Institute of Physics, University of Silesia in Katowice, SMCEBI, 75 Pułku Piechoty 1a, 41-500 Chorzów, Poland;

[2]Department of Laryngology, Medical University of Silesia, ul. Francuska 20-24, 40-027, Katowice, Poland

[3]School of Pharmacy and Pharmaceutical Sciences, Trinity College Dublin, College Green, Dublin 2, Ireland

[*]corresponding authors:

Abstract

In this article, the effect of mesoporous silica (MS) on the physical stability and molecular dynamics of the amorphous form of Celecoxib (CEL) is investigated. It has been proven that the recrystallization process of CEL slows down with increasing the MS content. Besides the elongation of stabilization time with the increase silica content leads to an increase in the amorphous drug fraction remaining after the finished crystallization. The conducted analyses show that the observed inhibition of CEL's recrystallization is associated with the formation of a monomolecular drug layer on the silica's surface. The performed non-isothermal dielectric studies of CEL + MS systems having both fully and partially amorphous CEL shows that the biggest impact of the drug's the temperature dependences of structural relaxation time $\tau_{\alpha}(T)$ has a crystalline fraction of the API. Silica, even in high concentration, does not modify the temperature dependence of structural relaxation of CEL.

Key words

Celecoxib, amorphous drug, physical stability, Syloid 244FP, molecular origin

1. Introduction

Most of the pharmaceutical products in the solid form contain a crystalline Active Pharmaceutical Ingredient (API). The principal advantage of this form is its high physical stability. However, as much as 40% of crystalline APIs are poorly soluble in water due to the presence of the crystal lattice.[1–3] Moreover, it is estimated that up to 90% of drug candidates in the crystalline form may be rejected during the research and development process just for this reason.[3,4] Taking into account that the solubility of an API is the limiting factor for its bioavailability, considerable effort is currently made to improve it.[5,6]

There are number of methods developed to enhance the water solubility of poorly soluble APIs. One of them is conversion of the crystalline form of drug to its amorphous counterpart.[7–9] As opposed to the crystal, in the amorphous state, there is no long-range ordering and consequently, an amorphous material has a larger internal energy. Due to this, weakening and/or breaking the intermolecular interactions is possible after delivering a lower energy compared to the crystal, where the energy levels are much higher. It means that substance in the amorphous form dissolves quicker and to a greater degree in water, often leading to better absorption of the substance in the human body.[10–12] However, amorphous substances are thermodynamically unstable.[13–15] As a consequence, they may recrystallize during storage and secondary manufacturing. The return to the crystalline form results in the loss of the beneficial properties resulting from the amorphous disorder. Therefore, it is necessary to find a method to effectively improve physical stability of amorphous APIs.[16–20]

Several strategies have been tested to establish the most efficient way of improving the physical stability of amorphous pharmaceuticals.[21–23] It appears that the use of mesoporous silica (MS) materials gives promising results.[24–26] MS has been shown to improve the physical stability of ibuprofen,[27,28] simvastatin,[29] ezetimibe[30] and nifedipine.[31] In addition to being highly effective in stabilizing amorphous forms of APIs, MS reduces the drug toxicity, have adequate biosafety (lack of cytotoxicity) and might be biodegradable.[32,33] All these features make these materials more and more attractive from the application point of view. Two possible mechanisms are commonly discussed to explain how MS can stabilize amorphous systems. If molecules of API are loaded into pores of MS, then the impeded crystallization might be related to the pore size effect. It means that if the pore diameter is smaller than the nucleus radius, it will result in a lack of recrystallization. The second mechanism is related to the specific interactions of drug molecules with the surface of MS.[34,35] However, we have shown recently that none of these mechanisms can be responsible for the stabilization of simvastatin with MS.[29] As discussed in our previous work, the stabilization effect was mainly

related to inhibition of the propagation of crystallization by using silica with appropriately small particle sizes. Since it has been demonstrated that a commercial grade of MS, Syloid 244FP (SYL244FP), with an average particle size of 2.5-3.7 μm and pore diameter of 23 nm gave the best stabilization result, in this work we carried out similar studies for another API, celecoxib (CEL). CEL was chosen due to its strong tendency toward recrystallization. In this context, the work of Grzybowska et al.[36] and Ajay et al.[37] are highlighted. The first paper describes in detail the dielectric response of amorphous CEL at both, supercooled liquid and glassy states. During the non-isothermal dielectric measurements performed in that work, cold crystallization with the onset at 365 K was observed. In the second paper the authors were mainly focused on investigating the isothermal crystallization of CEL from the supercooled liquid state. It has been shown that amorphous CEL at temperatures equal or higher than T = 363 K fully crystallized in less than 4 hours. The cited works confirm that amorphous CEL is highly thermodynamically unstable, therefore, it becomes an excellent candidate for our tests.

The aim of this study is as follows. Firstly, we wanted to investigate the effect of SYL244FP on the molecular dynamics of amorphous CEL. For that purpose, systems containing CEL and 9, 18, 27, 36 and 45 wt. % of SYL244FP were subjected to non-isothermal measurements using broadband dielectric spectroscopy (BDS). Secondly, we were interested in the impact of MS in the form of SYL244FP on the physical stability of amorphous CEL. To check the effect of the silica on recrystallization of CEL, neat API and its mixtures with SYL244FP were investigated applying isothermal (at T = 363 K) conditions using BDS. Finally, we wanted to discover which mechanism might be responsible for the observed CEL stabilization and to check whether CEL behaves similarly to simvastatin, for which a small amount of SYL244FP was sufficient to stabilize the drug effectively.

2. Materials and methods

2.1. Materials and preparation of mixtures

The crystalline form of celecoxib (CEL) with purity 98% and molecular mass M_w = 381 g/mol was purchased from Polpharma (Starogard Gdański, Poland). This pharmaceutical is chemically described as 4-[5-(4-methylphenyl)-3-(trifluoromethyl) pyrazol-1-yl] benzene-sulfonamide and belongs to a class of agents that selectively inhibit cyclooxygenase-2 (COX-2) enzymes. Its chemical structure is presented in the inset of Figure 1. Syloid 244 FP (SYL244FP) was received as a gift from Grace GmbH & CO. KG (Worms, Germany). This MS is characterized by average particle size of 2.5 – 3.7 μm, surface area of 314 m^2/g, pore

diameter ~23 nm and the pore volume equal to 1.6 mL/g. All chemicals were used as received.

To prepare the binary mixtures containing crystalline CEL and 9, 18, 27, 36 and 45 wt.% of SYL244, the weighted amounts of ingredients were mixed in a mortar for about 10 min. Every 3 minutes the sample was scraped off the mortar wall with a spatula. The prepared physical mixtures and neat SYL244FP were dried at 373 K for 10 min before experiments to remove water from MS, melted at T = 434 K and quenched directly before each experiment to obtain amorphous CEL in these mixtures. In the DSC experiments, the sample was vitrified *in situ* in the apparatus under dry nitrogen conditions, while for dielectric measurements, the melting procedure took place on the hot plate in air conditions with environmental humidity of approximately 25% RH.

2.2. Differential Scanning Calorimetry (DSC)

Thermal properties of neat CEL and its mixtures with SYL244FP were investigated using a Mettler−Toledo DSC 1 STAR^e System. The DSC was calibrated for temperature and enthalpy using zinc and indium standards. The instrument was equipped with an HSS8 ceramic sensor having 120 thermocouples and a liquid nitrogen cooling station. The samples were measured in aluminum crucibles (40 μL). All measurements were carried out with a heating rate of 10K/min.

2.3. Broadband Dielectric spectroscopy (BDS)

All dielectric measurements on neat CEL and its mixtures containing 9, 18, 27, 36 and 45 wt. % of SYL244FP were performed using Novo-Control GMBH Alpha dielectric spectrometer (Montabaur, Germany). The temperature in this apparatus was controlled by a Quattro temperature controller with temperature stability better than 0.1 K. Dielectric studies of fully amorphous samples were performed immediately after their vitrification by fast cooling of the melt in a parallel-plate cell made of stainless steel (diameter 15 mm and a 0.1 mm gap provided by silica spacer fibers). Dielectric experiments of partially amorphous CEL in systems with SYL244FP were performed ca. 12h after the cessation of crystallization. During non-isothermal studies of CEL + 9, 18, 27, 36, and 45 wt. % of SYL244FP, the dielectric spectra were registered in the temperature ranging from 173 to 383 K with a step of 2 K in a broad frequency range from 10^{-1} Hz to 10^6 Hz. During the non-isothermal high frequency study of neat CEL the dielectric loss spectra were measured at temperatures from 443 to 313 K with a step of 2 K for frequencies from 10^6 Hz to 10^9 Hz. The isothermal time-

dependent experiments for neat CEL and its mixtures with SYL244FP were performed at T = 363 K. The spectra were registered every 300s for a period of time after which lack of changes in dielectric spectrum were observed. During the non-isothermal studies of CEL + 9, 18, and 27 wt. % of SYL244FP with partially crystalline CEL, the dielectric spectra were registered at temperatures ranging from 333 to 433 K with a step of 10 K in a broad frequency range from 10^{-1} Hz to 10^{6} Hz.

3. Results and discussion

3.1. Thermal characterization of systems containing crystalline or amorphous CEL and SYL244FP

Thermal properties of neat CEL, SYL244FP, and its mixtures with 9, 18, 27, 36 and 45 wt. % of SYL244FP were investigated using DSC. Firstly, dry samples containing crystalline CEL were heated from 298 to 460 K. The heating procedure was carried out with a heating rate of 10 K/min. The obtained thermograms are presented in Figure 1. It can be seen that the DSC trace of neat crystalline CEL is characterized by one endothermal event corresponding to the drug melting. The melting temperature (T_m), which was determined as the onset of the endothermal process, is 434 K. This value agrees well with the literature. Interestingly, CEL in the presence of SYL244FP melts in two stages, i.e., on DSC thermograms two thermal events were recorded. The first peak has an onset at lower temperatures than the pure API (T_{m1}), while the second corresponds broadly to the melting temperature of neat CEL (T_{m2}), however some shift towards lower temperature is observed with an increasing amount of MS, consistent with the presence of MS as an impurity.[38] Also, the enthalpy of the second endothermic process decreases with an increasing amount of MS. At the same time an increase in enthalpy for the first process is observed. However, the appearance of the first endothermic process is unclear. It could be related to partially filling the pores of MS by the API or interactions of the drug molecules with the surface of MS[39,40]. However, the first scenario is unlikely due to the method of preparing the mixture, which was mechanical grinding CEL with Syloid244FP in a mortar. Therefore, in this case, the observed peak could be of another polymorphic form of CEL, i.e. form IV with a melt onset at 418–421 K [41] or it may be associated with interactions of the drug molecules with the surface of MS. Infrared spectroscopy (Figure 2) discounted the hypothesis of another polymorphic form, as all samples, included the one comprising 45 wt. % of SYL244FP and heated to 423 K, show the N-H stretching bands at the same positions, at 3335 and 3231 cm^{-1}. Lu and co-workers presented that CEL form IV had a different shape and position of those bands, at 3342, 3295

and 3213 cm^{-1}.[41] Spectroscopic studies also showed that no strong interactions between the MS and CEL are present in the mixtures with no changes to the bands of the sulfonamide functional group shown as the above N-H or S=O (at 1347 and 1159 cm^{-1}) stretching vibrations. The sulfonamide would be the group most likely to be involved in interactions with the Si-O-Si moieties (visible as a broad peak at 1200-1000 cm^{-1}). Therefore, the endothermic peak at app. 419 K in thermal analysis is most likely to be an artifact created by sample preparation, a comminution process, where the two components were ground together for 5 minutes, creating a variation in microstructure, similar to what was observed previously for itraconazole.[42] In addition, it appears that this intimate mixing may have generated opportunities for weaker interactions between CEL and SYL244FP, which were not discernible by infrared spectroscopy, to occur.

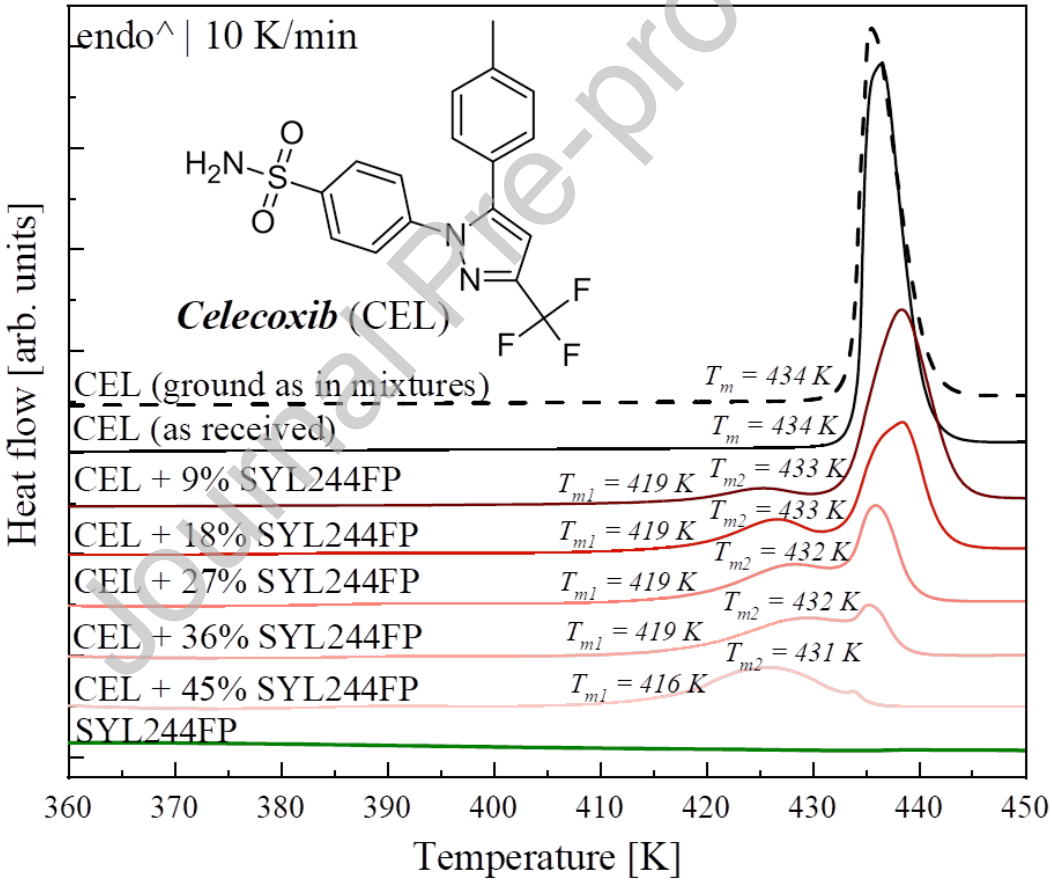

Figure 1. DSC thermograms of neat crystalline CEL, SYL244FP, and its physical mixtures with SYL244FP.

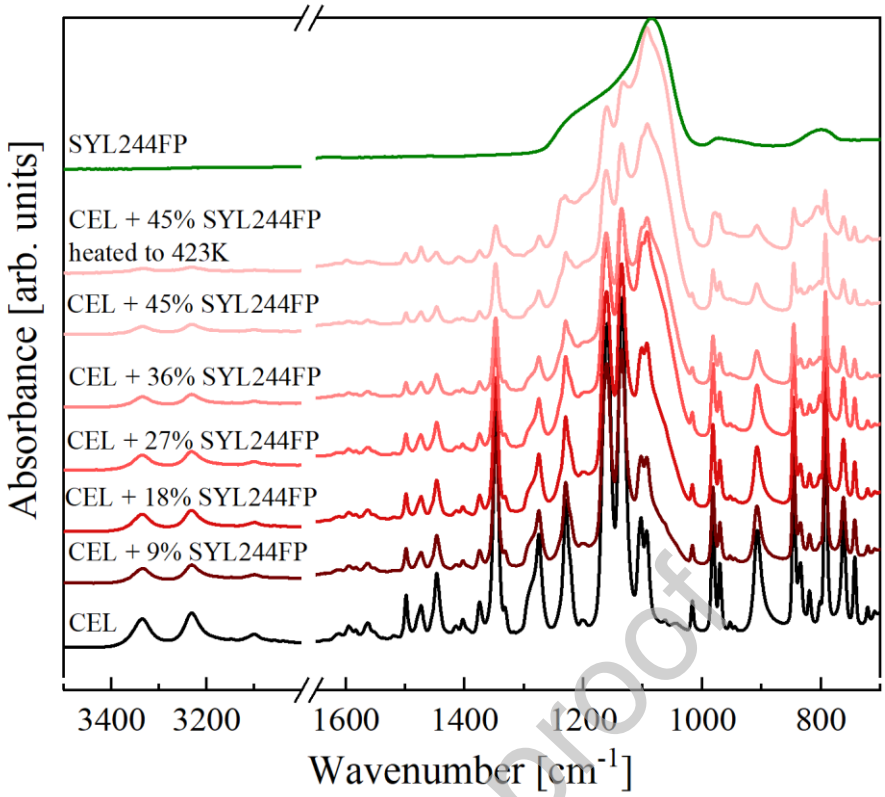

Figure 2. Infrared analysis of crystalline CEL and its mixtures with SYL244FP.

In the next step of calorimetric studies, the samples were quenched *in situ* in DSC to 273 K. The employed cooling rate was 20 K/min. No CEL crystallization was noted during this cooling stage. After the quenching, the samples were heated again, at 10 K/min, as used previously. The second heating thermograms presented of amorphous form of CEL (Figure 3). In the studied temperature range, only the step-like behavior, a manifestation of glass transition, was recorded on DSC thermograms. The glass transition temperature (T_g) was determined as a midpoint of the heat capacity increment and the values are shown in Figure 3. The presence of a single glass transition event confirms that CEL molecules do not fill the pores of SYL244FP. When the drug is incorporated inside the pores of silica, one should expect two T_gs. It is worth pointing out that the addition of SYL244FP did not change the value of CEL's glass transition temperature. This result is similar to our previous finding, where a lack of T_g modification in mixtures with SYL244FP was observed for simvastatin. With the increasing silica content one can however note a decrease in ΔC_p. Because the ΔC_p is an extensive and additive property, its value is proportional to the amorphous fraction of the system and will decrease linearly with decreasing drug content.[43] When molecules of amorphous API's fraction are absorbed to the MS surface does not contribute to any thermal event since they are "immobilized" by interactions with the functional groups of the surface

of MS. Consequently, if CEL molecules do not interact with the surface of MS, the value of ΔC_p of the mixture should proportionally decrease with the silica to zeros. If some interactions between CEL molecules and MS exist, a decrease in ΔC_p values should be larger than expected since the part of the amorphous fraction is "immobilized". Therefore, as Hempel et al. showed, by measuring the ΔC_p of various concentrations of drug + MS systems, it is possible to estimate the monomolecular loading capacity of the drug on the MS surface. [44]

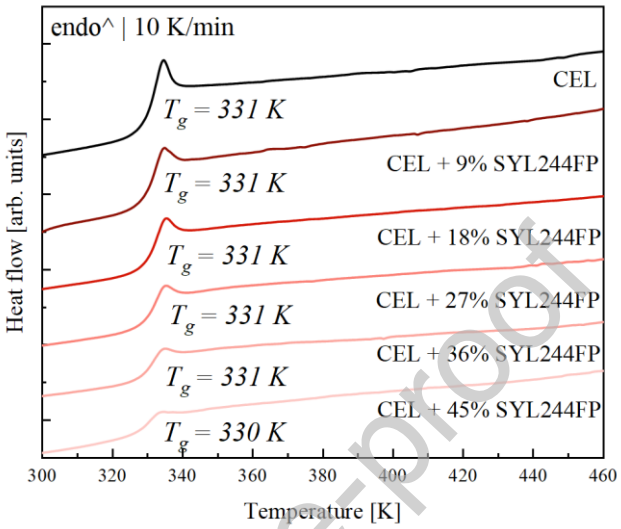

Figure 3. DSC thermograms of amorphous CEL and its mixtures with SYL244FP.

In order to determine the monomolecular loading capacity of CEL on the surface of SYL244FP the concentration dependence of ΔC_p for CEL + SYL244FP was prepared and is presented in Figure 4. The experimental data were fitted to a linear function and from its extrapolation to ΔC_p = 0 the monomolecular loading capacity was determined as 13.5 wt. % of CEL.

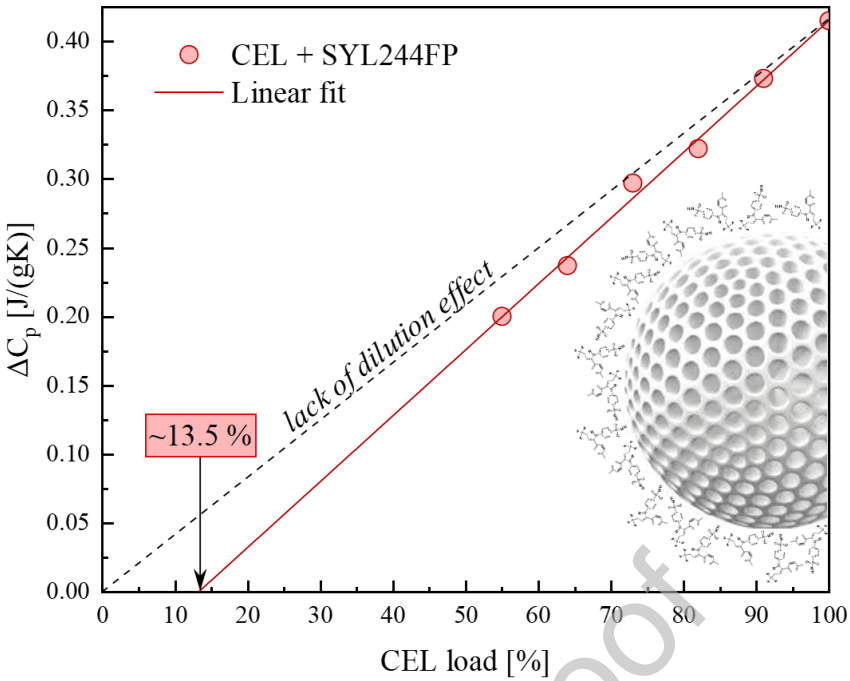

Figure 4. Linear extrapolation of the ΔC_p values as a function of drug loading.

3.2. Molecular dynamics of CEL + SYL244FP systems

In this part of paper, the effect of MS on the molecular dynamics of CEL is investigated. The molecular dynamics studies of the quenched CEL + SYL244FP systems were performed by BDS. The non-isothermal dielectric loss spectra measurements were performed in a broad frequency (from 10^{-1} to 10^{6} Hz) and temperature range (from 173 to 383 K). Figure 5 a-e shows the representative dielectric loss spectra obtained above T_g for CEL + SYL244FP systems with different silica concentration. In the low frequency region a characteristic contribution from DC-conductivity can be identified. However, the most significant process in $\varepsilon''(\omega)$ is the structural (α) relaxation process. Increasing the temperature leads to shifting of α-relaxation peak towards higher frequencies, reflecting enhancement of molecular mobility. It is worth highlighting that during non-isothermal dielectric measurements, one can observe a cold crystallization process for systems at concentrations of SYL244FP of 27 wt. % or lower. The beginning of crystallization for these systems occurred at 369 K for systems with 9 and 18 wt. % of SYL244FP, and at 371 K for the system with 27 wt. % of SYL244FP. The recrystallization process is manifested by a rapid decrease in the intensity of the dielectric loss peak of α – process (see light-red dashed lines in Figure 5 a-e).[45] The drop in the intensity of the peak is due to the fact that the population of reorienting polar molecules decreases as the crystallization progresses. Note that the intensity of the α – peak, $\Delta\varepsilon_\alpha$, is proportional to $N\mu^2$, where N is a number of reorienting dipoles and μ is the value

of dipole moment of molecule. For the samples containing 36 and 45 wt.% of SYL244FP, crystallization was not observed during the measurement, proving that the presence of silica improves the physical stability of CEL.

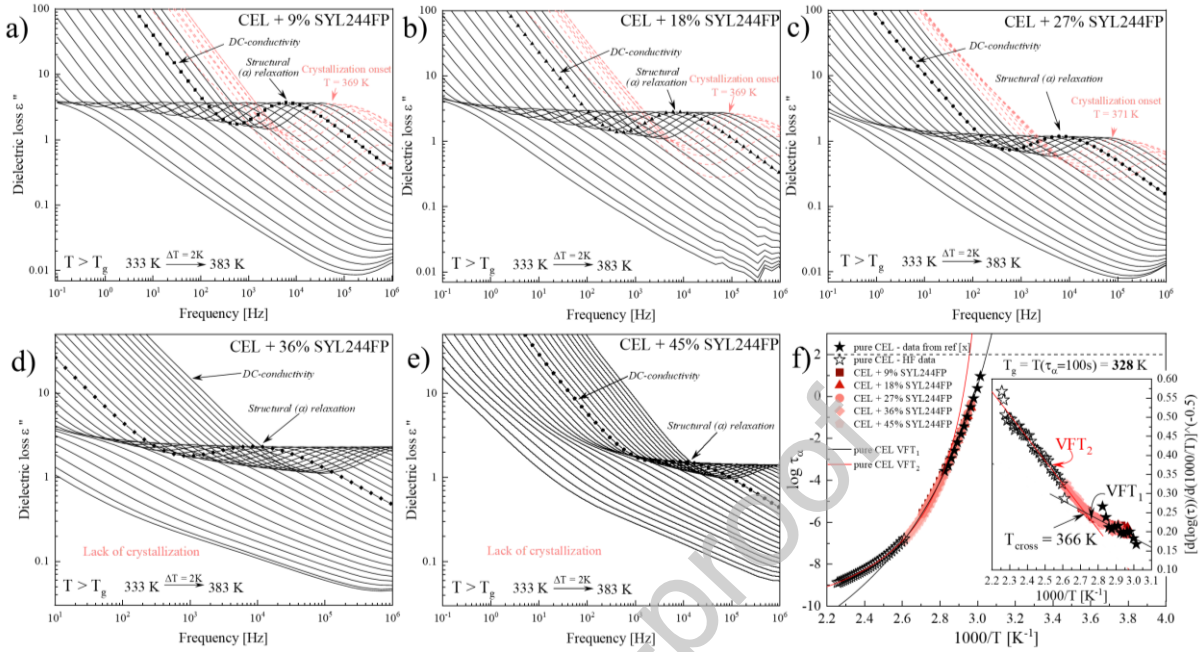

Figure 5. Dielectric loss spectra of CEL + SYL244FP containing: (a) 9% of silica, (b) 18% of silica, (c) 27% of silica, (d) 36% of silica and (e) 45% of silica. The spectra were collected upon heating at T > T_g. In panel (f), the temperature dependence of τ_α for all tested systems are compared to $\tau_\alpha(T)$ of neat CEL (data from the low temperature region presented as filled stars were taken from ref. [36], while those from the high temperature region, presented as empty stars, were taken from the high frequency experiment). The inset of panel (f) shows the result of the derivative analysis focused on the validity of VFT parameterization. The intersection of the two VFT lines denotes the crossover temperature T_{cross} = 366 K.

The dielectric loss spectra of all studied systems were analyzed to obtain values of the structural relaxation times (τ_α). For this purpose the dielectric loss spectra were fitted by the Havriliak-Negami (HN) function with an additional term describing the DC-conductivity contribution:[46]

$$\varepsilon^*(\omega) = \varepsilon_\infty + \frac{\Delta\varepsilon}{[1+(i\omega\tau_{HN})^a]^b} + \frac{\sigma_{dc}}{\varepsilon_0 i\omega} \quad (1)$$

where ε_∞ is the high-frequency limit permittivity, ε_0 signify the permittivity of vacuum, $\Delta\varepsilon$ is dielectric strength, ω is equal to $2\pi f$, τ_{HN} is the HN relaxation time, and a and b represent symmetric and asymmetric broadening of the relaxation peak. From the fitting parameters we then determined values of τ_α using the following formula:

$$\tau_\alpha = \tau_{HN}[sin(\frac{\pi a}{2+2b})]^{\frac{1}{a}}[sin(\frac{\pi ab}{2+2b})]^{-\frac{1}{a}} \quad (2)$$

The temperature evolutions of the structural relaxation times of both neat CEL as well as its mixtures with SYL244FP are depicted in Figure 5f. The data for neat CEL, which are marked as black filled stars, were taken from the publication of Grzybowska et al.[36] In order to parameterize the experimental data the Vogel-Fulcher-Tammann (VFT) equation was employed:[47–49]

$$\tau_\alpha(T) = \tau_\infty \, exp(\frac{DT_0}{T-T_0}) \quad (3)$$

where τ_∞, T_0, and D, are fitting parameters. Parameter τ_∞ is a pre-exponential factor denoting the upper limit of temperature for τ_α, and its value should be of order of around 10^{-14} s (i.e. vibrational frequency of molecule). T_0 is the Vogel temperature, which corresponds to the state with infinite relaxation time, and D denotes deviation from the Arrhenius model. During the analysis we noticed that the temperature evolution of the structural relaxation time of systems with concentrations of SYL244FP greater than 27 wt. % is not consistent over the entire experimental temperature range to fit to a single VFT equation. Therefore, the detailed analysis of the temperature dependence of τ_α were performed. For that purpose, the derivative method proposed by Stickel was employed.[50] According to this method, a plot of the values of the derivative operator $[-dlog(\tau_\alpha)/dT]^{(-0.5)}$ versus temperature should be linear for a single VFT function. Since two distinct linear regions are observed for CEL + 36% SYL244FP and CEL + 45% SYL244FP, two sets of VFT fitting parameters are required to describe the data over the entire temperature range. It is worth pointing out that in the case of neat CEL there is no information in the literature about the requirement of using two VFT. Thus, the question arises: *why in the mixtures such a behavior was noted?* There are two possible reasons. The silica used in our experiments might either modify the temperature dependence of τ_α of the drug or due to stabilization effect SYL244FP might reveal true nature of CEL $\tau_\alpha(T)$. To verify whether the silica changes or not the $\tau_\alpha(T)$ of CEL, an additional experiment was performed by means of a high frequency setup for BDS. During this experiment, to avoid recrystallization, the sample was measured on cooling from 443 to 383 K with a step of 2 K. The temperature dependence of $\tau_\alpha(T)$ for the neat API determined based on the analysis of these data is presented in Figure 5f as the empty stars. The Stickel analysis indicated that two sets of VFT fitting parameters are required to describe the data of neat CEL over the entire temperature range. The intersection of these two VFT lines, seen in the inset of Figure 5f, gives a crossover temperature T_{cross} = 366 K.[51] This result proves that SYL244FP does not modify the temperature dependence of CEL structural relaxation time but due to the drug stabilization elongates the available for measurement frequency window. Since different

mixtures of SYL244FP with CEL exhibit the same temperature dependencies as neat CEL, their glass transition temperatures are identical. To determine T_g of neat CEL and its mixtures with SYL244FP the VFT_1 functions were extrapolated to the value of τ_α = 100s (T_g = T (τ_α = 100s) = 328 K). The T_g values determined by BDS are consistent with the data obtained from calorimetric measurements. Slight discrepancies result from the different heating rates applied during the calorimetric (*HR* = 10 K/min) and dielectric (*HR* = 0.5 K/min) measurements.

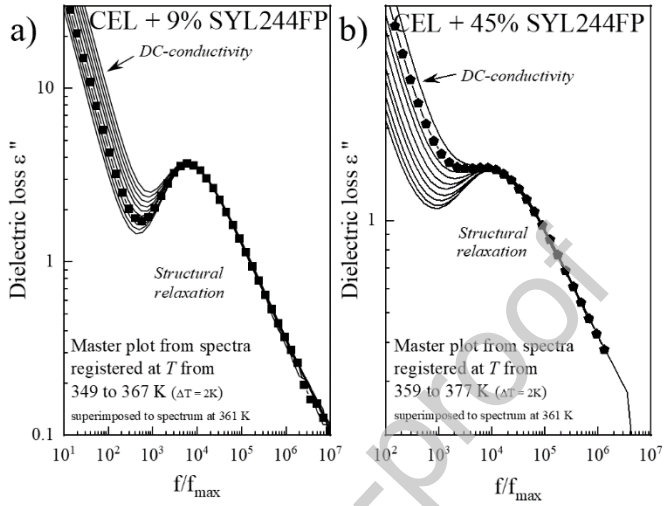

Figure 6. The master plot from dielectric loss spectra of: (a) CEL + 9 % of SYL244FP, and SVT + 45 % of SYL244 formed by horizontal shifting of spectra to overlap the reference system.

In the next step of analysis of the dielectric loss spectra, we concentrated on the shape of the α – process. Firstly, we checked if the shape of the α – process changes with temperature. In order to do this, we constructed for each composition a master plot, i.e.: the reference spectrum was selected and remaining spectra were shifted along horizontal and vertical axes to superimpose them on the reference system. The master plots for the extreme MS concentrations are presented in Figure 6. It can be seen that, with exception of an increase in DC-conductivity with decreasing temperature, the shape of the structural relaxation process does not change in a given temperature range for the CEL + SYL244FP systems. It now becomes interesting to test if the shape of the structural relaxation peak is dependent on the concentration of SYL244FP. To perform a more quantitative analysis, we used the Kohlrausch–Williams–Watts (KWW) function to fit the α – relaxation peak. The advantage of using this fitting function is that it has only a single parameter, β_{KWW}, characterizing the shape of the relaxation curve.[52] Its value can change from 0 to 1, with a value of 1 indicating that the alpha relaxation peak is narrow and symmetrical, which corresponds to the Debye case. As the value of β_{KWW} decreases towards 0 the peak becomes broader and asymmetric. The results

of the shape analysis of the structural relaxation peak in terms of the KWW function are presented in Figure 7. It becomes obvious that the value of the β_{KWW} parameter decreases with the increasing concentration of SYL244FP. For instance, Shamblin et al. noticed that for materials with low β_{KWW} values the tendency to crystallization is much higher.[53] This phenomenological observation disagrees with our finding as for systems with the lowest β_{KWW} values (i.e., higher concentration of SYL244FP) crystallization was not observed during the non-isothermal dielectric measurements. Note that the similar discrepancy between the physical stability of amorphous API and its β_{KWW} value has been previously observed for other pharmaceuticals, i.e. ezetimibe and sildenafil. Furthermore, in our case, broadening the α-relaxation peak of CEL is associated with the increase of the system heterogeneity.[54]

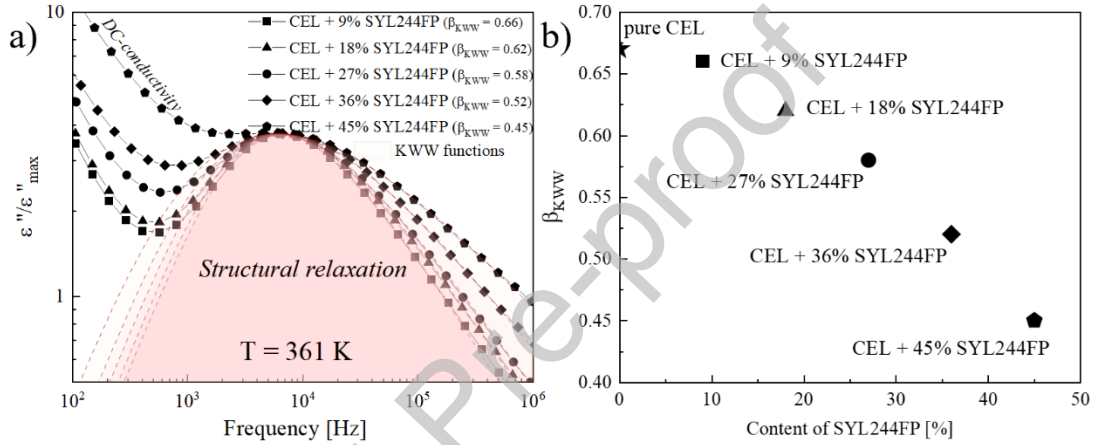

Figure 7. (a) Comparison of the dielectric spectra of various concentrations of the CEL + SYL244FP systems recorded at T = 361 K. The dashed lines represent the KWW fit to the *α*-peak with a value of β_{KWW} given in the legend. (b) The concentration dependence of β_{KWW} for the CEL + SYL244FP systems.

3.3. Studies of the effect of silica additive on the physical stability of amorphous CEL

Presented in the previous section, non-isothermal dielectric studies indicated that SYL244FP improves the physical stability of amorphous CEL. However, based on these data, it is impossible to assess the stabilization effect. Therefore, to properly evaluate the effectiveness of SYL244FP in the stabilization of the disordered form of CEL, time-dependent, isothermal dielectric studies were performed. The crystallization of both neat CEL and its mixture with SYL244FP was measured at T = 363 K (the spectra were registered every 300s). This particular temperature was selected for two reasons. Firstly, the crystallization kinetics of neat CEL was previously investigated by Dantuluri et. al at temperatures ranging from 363 to 378 K (ΔT = 5 K).[37] Thus, choosing one of these temperature conditions, one can check whether the investigated by us batch of the drug behave identically as that shown in the literature. Secondly, at T = 363 K neat CEL should fully convert to its crystalline form after

ca. 4h. This period of time is on the one hand long enough to safely prepare and measure the sample avoiding partial crystallization, while on the other hand, fast enough to investigate how the silica stabilizes the drug.

Figure 8 shows the representative (i.e., registered every 1200s), data obtained for neat CEL. It can be seen that the crystallization process can be followed directly in both the real (ε') and imaginary (ε'') parts of the complex dielectric permittivity, reflected by a decrease of the static permittivity (ε_s) and an increase in the intensity of the loss peak with time, respectively.[55]

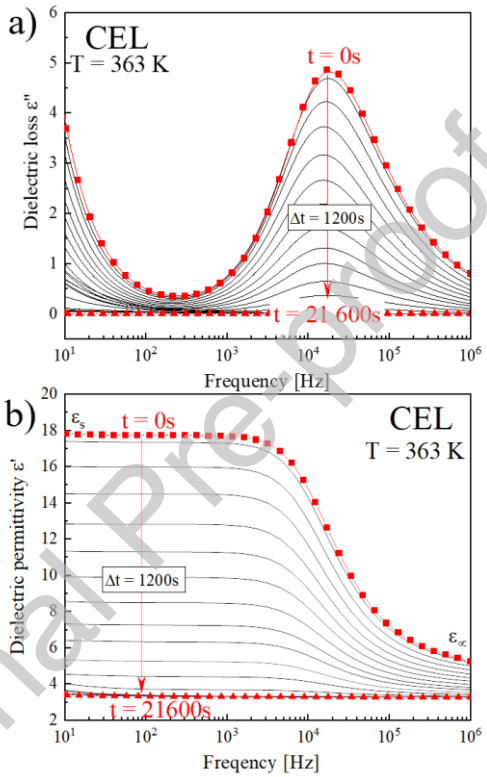

Figure 8. Dielectric spectra of the imaginary (upper panel) and real (lower panel) parts of the complex dielectric permittivity during an isothermal crystallization of neat CEL at *T* = 363 K.

However, since usually the progress of crystallization is analyzed in terms of the normalized real permittivity (ε'_N), in the further part of this work we will present data only in the dielectric permittivity representation. The aforementioned ε'_N is defined as:[56]

$$\varepsilon_N' = \frac{\varepsilon'(0)-\varepsilon'(t)}{\varepsilon'(0)-\varepsilon'(\infty)} \quad (4)$$

where $\varepsilon'(0)$ is the initial static dielectric permittivity, $\varepsilon'(\infty)$ is the long-time limiting value, and $\varepsilon'(t)$ is the value at time t. Normalized by this method data of neat CEL were compared to the crystallization kinetics of CEL obtained from digitalizing the data from the Dantuluri et al. paper.[37] Both time dependences are plotted together as empty and filled circles in Figure 10a.

Since the kinetics of CEL crystallization measured by us is identical as that investigated earlier, we can conclude that the sample batch has no impact on the physical stability of this API and one can investigate the effect of silica on its stabilization. For this purpose, the systems containing CEL and 9, 18, 27, 36 and 45 wt. % of SYL244FP were isothermally measured at T = 363 K by means of BDS (Δt = *300s*). The representative spectra obtained from these experiments (i.e., with Δt = *1200s*, Δt = *2400s*, and Δt = *3600s* for CEL + 9% SYL244FP, CEL + 18% SYL244FP, and CEL + 27% SYL244FP, respectively) are presented in Figure 9a-c.

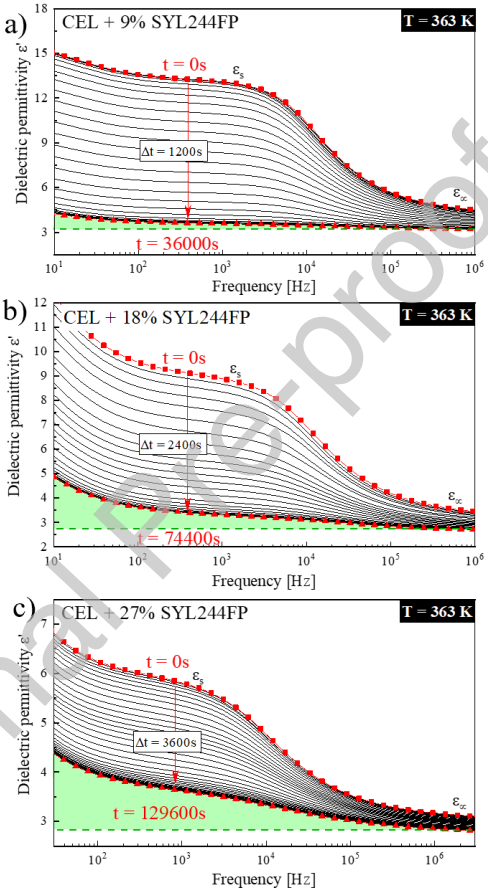

Figure 9. Dielectric spectra of the real part of the complex dielectric permittivity during an isothermal crystallization at T = 363 K of (a) CEL + 9% SYL244FP, (b) CEL + 18% SYL244FP, and (c) CEL + 27% SYL244FP.

Note that, since SYL244FP does not modify the temperature dependence of τ_α of neat CEL, these experiments were performed not only at fixed temperature conditions but also at constant τ_α, i.e., isothermal conditions. A drop in the static permittivity (ε_s) was observed during all experiments indicating that CEL recrystallizes from the drug-silica binary systems, even when high SYL244FP content is employed. However, crystallization observed in CEL mixtures is unfinished, and its degree decreases with the increasing amount of SYL244FP

(see the green areas in Figure 9a-c). The end of the crystallization process was considered when no further changes in the dielectric spectrum were observed. To properly analyze these data, i.e., to take into account the degree of CEL crystallization, we took the value of ε_∞ instead of $\varepsilon'(\infty)$ in eq. 4. The comparison of all kinetic curves is presented in Figure 10a. As can be seen by increasing the amount of the silica, the prolongation of the CEL recrystallization was noted indicating that SYL244FP improves the physical stability of amorphous CEL. It is worth pointing out that a similar partial crystallization of the drug measured by means of BDS was previously observed when API was mixed with another drug (drug-drug system)[57] or polymer (drug-polymer system)[58–60]. In these cases, together with the reduction of $\Delta\varepsilon$, the shift in the position of the structural relaxation process was noted proving that the molecular dynamics of the system was changing. The incomplete crystallization of the drugs described in the mentioned works results from the crystallization of the excess of drug from the supersaturated system (drug-drug or drug-polymer). Thus, this allows to determine the concentration corresponding to the saturated system, which should guarantee high physical stability. However, such scenario is impossible for the CEL + SYL244FP systems since the drug cannot be dissolved in the silica.

By analyzing the kinetic curves, the crystallization half-life time ($t_{1/2}$) and the degree of CEL crystallinity were determined. The obtained values are summarized in Figure 10b. The concentration dependence of the degree of CEL crystallinity shows a linear behavior. Therefore, by extrapolating the fitted to these data a linear function to 0% of CEL crystallinity, one can predict what concentration of the silica is needed to fully stabilize the amorphous form of the investigated drug. Based on this analysis, one can estimate that at least 85.3 wt. % of SYL244FP is needed to fully prevent crystallization of the API. Note that this concentration corresponds well (±1%) with concentration in which CEL molecules form the monomolecular layer on the silica surface (i.e., 86.5 wt. %), as determined above from the calorimetric studies. This result suggests that SYL244FP inhibits only the crystallization of CEL molecules located nearby the surface of the silica. Based on this assumption one can conclude that the observed stabilization of CEL in the systems with SYL244FP originates from the interaction of drug molecules with the surface of the silica.

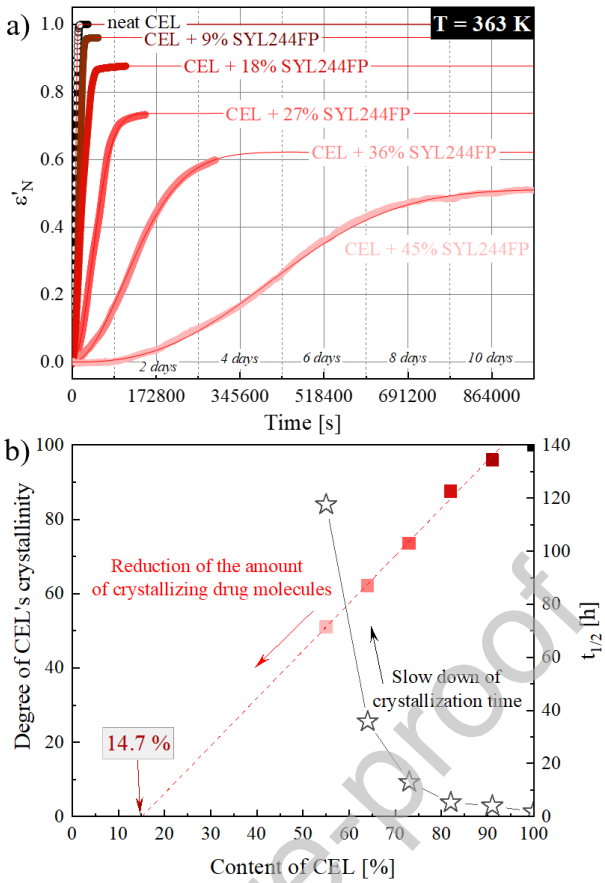

Figure 10. Panel (a) compares the time dependences of ε_N' for neat CEL (empty circles – data from ref [37], filled circles – data from our experiment), and its mixtures with 9, 18, 27, 36 and 45% of SYL244FP at 363 K. Panel (b) shows presented as a squares the concentration dependence of degree of CEL crystallinity obtained after the isothermal dielectric studies and presented as a stars concentration dependence of CEL crystallization half-life time from the mixtures with SYL244FP.

3.4. Molecular dynamics of recrystallized CEL + SYL244FP systems

In the previous section, it was shown that CEL remains partially amorphous after recrystallization from the mixtures with SYL244FP. The samples obtained after the isothermal BDS experiments (where crystallization was observed) were again subjected to non-isothermal dielectric studies. These tests were performed for two reasons. On the one hand, they can prove whether or not the amorphous fraction of CEL still remains in the CEL + SYL244FP systems. While on the other hand, these experiments will show how the molecular dynamics of the investigated systems change when some part of CEL converts to the crystalline form.

The dielectric loss spectra of partially amorphous systems containing 9, 18 and 27 wt. % of SYL244FP were measured at temperatures from 333 to 433 K (ΔT = 10 K). The representative dielectric loss spectra are presented in Figure 11 a and b. The investigated

systems reveal two processes. One is located at higher frequencies reflecting the structural relaxation associated with the CEL glass transition dynamics, while the second i.e., slower process, is probably associated with the Maxwell-Wagner-Sillars (MWS) polarization mechanism.[61–63] MWS processes reflect the trapping and accumulation of charges at the interface of the different phases of the sample. Considering that in the measured samples three different phases exists (i.e., crystalline CEL, amorphous CEL and SYL244FP) the origin of this process seems to be obvious. However, it can also originate from the dynamic of CEL molecules localized nearby the pore walls and/or the crystallite front. In order to determine the temperature evolution of the structural and "slow" processes, the dielectric loss spectra were fitted in a similar way to that used for the fully amorphous systems with two HN functions used instead of one. An exemplary fit of spectra investigated at T = 363 K for CEL containing 9, 18 and 27 wt. % of SYL244FP are presented in Figure 11c. The intensity of the process located at lower frequencies increases with the increasing the silica content. This suggests that the "slower" process indeed reflects the MWS polarization. It is well known that MWS effects are more pronounced for conductive materials. This is consistent with the obtained data – as shown in Figure 7a, conductivity of the mixture increases with the increasing SYL244FP content. If the "slower" process originated from the dynamics of the interfacial CEL molecules, a reduction of the process intensity with the increasing SYL244FP would be visible. It is because a reduction in the crystalline fraction was noted with increasing silica content consistent with a smaller surface area of the crystal.

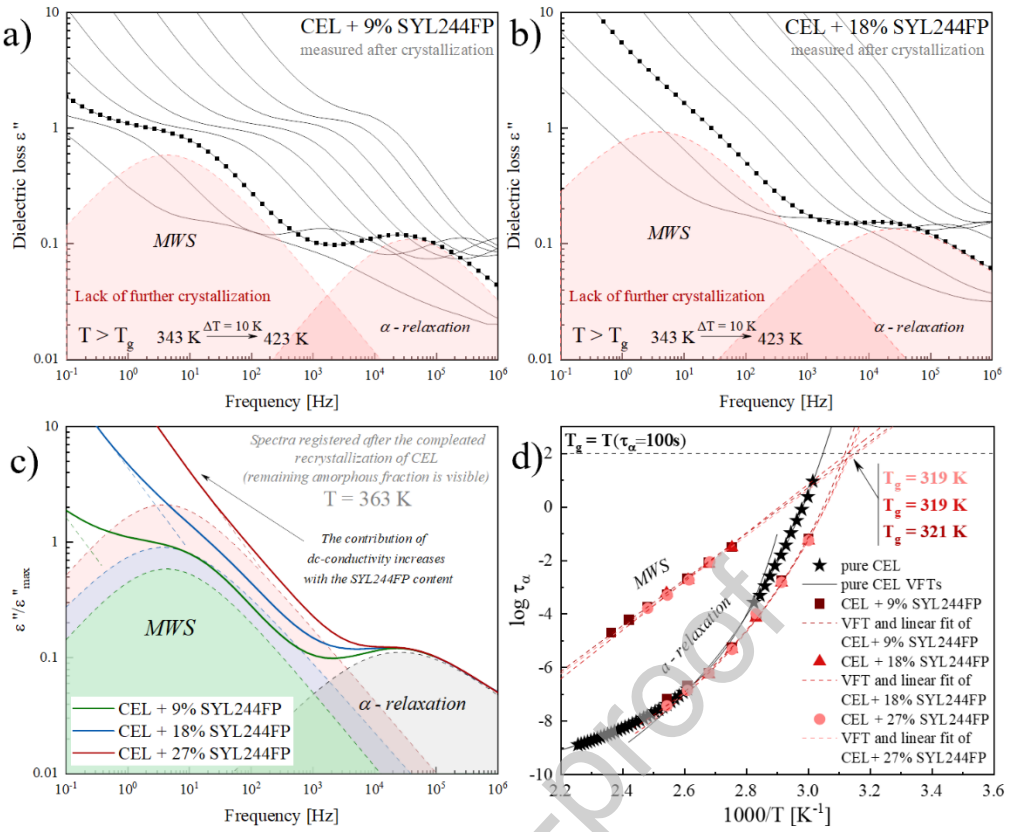

Figure 11. Dielectric loss spectra of samples obtained after time-dependent isothermal dielectric studies which contain crystalline and amorphous fractions of CEL and (a) 9% of SYL244FP and (b) 18% of SYL244FP. Panel (c) compares the dielectric loss spectra of partially crystalline CEL + SYL244FP systems registered at T = 363 K. In panel (d), the temperature dependences of τ_α and τ_{MWS} of all tested systems are compared to $\tau_\alpha(T)$ of neat CEL.

The values of τ_α, and τ_{MWS} were determined from the obtained fitting parameters. The $\tau_\alpha(T)$, and $\tau_{MWS}(T)$ of the measured systems are compared to $\tau_\alpha(T)$ of neat CEL in Figure 11d. The MWS process of all investigated systems reveals an Arrhenius *T* dependence, while the temperature dependence of CEL structural relaxation time in the partially amorphous systems follows VFT behavior. It is clear that the latter dependences differ (especially at the low temperature region) from $\tau_\alpha(T)$ of neat CEL and consequently from $\tau_\alpha(T)$ of amorphous CEL in mixtures with SYL244FP. To describe the temperature evolution of τ_α of mixtures with partially amorphous CEL, the VFT equation (eq. 3) was employed. The comparison of VFT fitting parameter of systems containing partially amorphous CEL and neat CEL are shown in Table 1. The glass transition temperatures of the investigated systems, which were determined from the fit extrapolation, are 321 K for CEL + 9% SYL244FP, and 319 K for CEL + 18% SYL244FP as well as CEL + 27% SYL244FP. It should be stressed that the presence of the α

– relaxation process in the recorded spectra demonstrates that part of CEL indeed remains amorphous in the investigated samples.

Sample	$\log_{10}(\tau_\infty/s)$	$B = DT_0$	T_0
neat CEL	-13.97 ± 0.04	1 758.3 ± 11.6	280.2 ± 0.8
CEL + 9% SYL244FP	-14.4 ± 0.56	2044.3 ± 54.4	266.5 ± 2.1
CEL + 18% SYL244FP	-15.72 ± 0.98	2555.5 ± 48.2	256.7 ± 1.7
CEL + 27% SYL244FP	-15.87 ± 1.48	2698.0 ± 78.5	253.1 ± 3.1

Table 1. Comparison of the VFT_1 parameters of neat, fully amorphous CEL and partially crystalline CEL in mixtures with 9, 18 and 27% of SYL244FP.

4. Conclusions

In this paper we investigated the impact of MS in the form of SYL244FP on the molecular dynamics and physical stability of amorphous CEL. For that purpose, a series of calorimetric and dielectric studies of various concentrations of CEL + SYL244FP were performed. As the calorimetric data shows, the presence of SYL244FP significantly modifies the melting process of CEL resulting in the drug melting in two stages. Interestingly, SYL244FP have no impact on the glass transition temperature of the API. From the analysis of the change in specific heat capacity of glass transition temperature process of the CEL + silica systems, the monomolecular loading capacity of CEL on the silica surface was determined as 13.5 wt. %. Non-isothermal dielectric studies of systems containing fully amorphous CEL and SYL244FP show that the silica did not modify the temperature dependence of the structural relaxation time of the API. It however has an impact on the distribution of the structural relaxation peak. With the increasing amount of the silica in the system, the α – relaxation peak of CEL becomes broader. Subsequent isothermal BDS experiments showed that the increased content of SYL244FP in CEL mixtures causes prolongation of the drug recrystallization time as well as it leads to an increase in the amount of the drug remaining stable in the amorphous form. The analysis of the degree of crystallinity of the samples in which completed crystallization was observed suggests that SYL244FP inhibits crystallization of CEL molecules located only nearby the surface of the silica. Based on this observation it can be concluded that the observed stabilization of CEL originates from interactions of drug molecules with the surface of the silica. Finally, the molecular dynamics of the systems with partially amorphous CEL were investigated. The dielectric loss spectra of the systems with only partially amorphous CEL reveals an extra process in addition to the α-relaxation peak. Due to the high inhomogeneity of these systems this process was identified as the MWS polarization.

Dielectric studies of these complex systems confirmed that indeed a fraction of CEL remains amorphous in the sample and the presence of the crystalline fraction of the CEL in the system modifies the $\tau_\alpha(T)$ of the drug.

5. Funding

This research was funded by the National Science Centre (Poland), Project No. 2018/31/B/ST8/01327 (OPUS 16).

6. Acknowledgements

The authors thanks Beibei Yao (University of Silesia) for carrying out additional measurements for pure celecoxib using high frequency dielectric spectroscopy.

7. References

(1) Fahr, A.; Liu, X. Drug Delivery Strategies for Poorly Water-Soluble Drugs. *Expert Opin. Drug Deliv.* **2007**, *4* (4). https://doi.org/10.1517/17425247.4.4.403.

(2) Williams, H. D.; Trevaskis, N. L.; Charman, S. A.; Shanker, R. M.; Charman, W. N.; Pouton, C. W.; Porter, C. J. H. Strategies to Address Low Drug Solubility in Discovery and Development. *Pharmacol. Rev.* **2013**, *65* (1), 315–499. https://doi.org/10.1124/pr.112.005660.

(3) Babu, N. J.; Nangia, A. Solubility Advantage of Amorphous Drugs and Pharmaceutical Cocrystals. *Cryst. Growth Des.* **2011**, *11* (7), 2662–2679. https://doi.org/10.1021/cg200492w.

(4) Kalepu, S.; Nekkanti, V. Insoluble Drug Delivery Strategies: Review of Recent Advances and Business Prospects. *Acta Pharm. Sin. B* **2015**, *5* (5), 442–453. https://doi.org/10.1016/j.apsb.2015.07.003.

(5) Vasconcelos, T.; Sarmento, B.; Costa, P. Solid Dispersions as Strategy to Improve Oral Bioavailability of Poor Water Soluble Drugs. *Drug Discov. Today* **2007**, *12* (23–24), 1068–1075. https://doi.org/10.1016/j.drudis.2007.09.005.

(6) Cid, A. G.; Simonazzi, A.; Palma, S. D.; Bermúdez, J. M. Solid Dispersion Technology as a Strategy to Improve the Bioavailability of Poorly Soluble Drugs. *Ther. Deliv.* **2019**, *10* (6), 363–382. https://doi.org/10.4155/tde-2019-0007.

(7) Baird, J. A.; Taylor, L. S. Evaluation of Amorphous Solid Dispersion Properties Using Thermal Analysis Techniques. *Adv. Drug Deliv. Rev.* **2012**, *64* (5), 396–421. https://doi.org/10.1016/j.addr.2011.07.009.

(8) Hancock, B. C.; Parks, M. What Is the True Solubility Advantage for Amorphous Pharmaceuticals? **2000**, *17* (4), 397–404. https://doi.org/10.1023/A:1007516718048.

(9) Bogner, R. H.; Murdande, S. B.; Pikal, M. J.; Shanker, R. M. Solubility Advantage of Amorphous Pharmaceuticals: II. Application of Quantitative Thermodynamic Relationships for Prediction of Solubility Enhancement in Structurally Diverse Insoluble Pharmaceuticals. *Pharm. Res.* **2010**, *27* (12), 2704–2714. https://doi.org/10.1007/s11095-010-0269-5.

(10) Hancock, B. C.; Zografi, G. Characteristics and Significance of the Amorphous State in Pharmaceutical Systems. *J. Pharm. Sci.* **1997**, *86* (1), 1. https://doi.org/10.1021/js9601896.

(11) Kawakami, K. Modification of Physicochemical Characteristics of Active Pharmaceutical Ingredients and Application of Supersaturatable Dosage Forms for Improving Bioavailability of Poorly Absorbed Drugs. *Adv. Drug Deliv. Rev.* **2012**, *64*

(6), 480–495. https://doi.org/10.1016/j.addr.2011.10.009.
(12) Hu, L.; Tang, X.; Cui, F. Solid Lipid Nanoparticles (SLNs) to Improve Oral Bioavailability of Poorly Soluble Drugs. *J. Pharm. Pharmacol.* **2010**, *56* (12), 1527–1535. https://doi.org/10.1211/0022357044959.
(13) Kothari, K.; Ragoonanan, V.; Suryanarayanan, R. Influence of Molecular Mobility on the Physical Stability of Amorphous Pharmaceuticals in the Supercooled and Glassy States. *Mol. Pharm.* **2014**, *11* (9), 3048–3055. https://doi.org/10.1021/mp500229d.
(14) Szklarz, G.; Adrjanowicz, K.; Knapik-Kowalczuk, J.; Jurkiewicz, K.; Paluch, M. Crystallization of Supercooled Fenofibrate Studied at Ambient and Elevated Pressures. *Phys. Chem. Chem. Phys.* **2017**, *19* (15), 9879–9888. https://doi.org/10.1039/c7cp00823f.
(15) Karmwar, P.; Graeser, K.; Gordon, K. C.; Strachan, C. J.; Rades, T. Investigation of Properties and Recrystallisation Behaviour of Amorphous Indomethacin Samples Prepared by Different Methods. *Int. J. Pharm.* **2011**, *417* (1–2), 94–100. https://doi.org/10.1016/j.ijpharm.2010.12.019.
(16) Knapik, J.; Wojnarowska, Z.; Grzybowska, K.; Jurkiewicz, K.; Tajber, L.; Paluch, M. Molecular Dynamics and Physical Stability of Coamorphous Ezetimib and Indapamide Mixtures. *Mol. Pharm.* **2015**, *12* (10), 3610–3619. https://doi.org/10.1021/acs.molpharmaceut.5b00334.
(17) Kawakami, K. Ultraslow Cooling for the Stabilization of Pharmaceutical Glasses. *J. Phys. Chem. B* **2019**, *123* (23), 4996–5003. https://doi.org/10.1021/acs.jpcb.9b02122.
(18) Baghel, S.; Cathcart, H.; O'Reilly, N. J. Polymeric Amorphous Solid Dispersions: A Review of Amorphization, Crystallization, Stabilization, Solid-State Characterization, and Aqueous Solubilization of Biopharmaceutical Classification System Class II Drugs. *J. Pharm. Sci.* **2016**, *105* (9), 2527–2544. https://doi.org/10.1016/j.xphs.2015.10.008.
(19) Knapik-Kowalczuk, J.; Tu, W.; Chmiel, K.; Rams-Baron, M.; Paluch, M. Co-Stabilization of Amorphous Pharmaceuticals - The Case of Nifedipine and Nimodipine. *Mol. Pharm.* **2018**, *15* (6), 2455–2465. https://doi.org/10.1021/acs.molpharmaceut.8b00308.
(20) Khanfar, M.; Al-Nimry, S. Stabilization and Amorphization of Lovastatin Using Different Types of Silica. *AAPS PharmSciTech* **2017**, *18* (6), 2358–2367. https://doi.org/10.1208/s12249-017-0717-1.
(21) Laitinen, R.; Löbmann, K.; Strachan, C. J.; Grohganz, H.; Rades, T. Emerging Trends in the Stabilization of Amorphous Drugs. *Int. J. Pharm.* **2013**, *453* (1), 65–79. https://doi.org/10.1016/j.ijpharm.2012.04.066.
(22) Singh, A.; Worku, Z. A.; Van Den Mooter, G. Oral Formulation Strategies to Improve Solubility of Poorly Water-Soluble Drugs. *Expert Opin. Drug Deliv.* **2011**, *8* (10), 1361–1378. https://doi.org/10.1517/17425247.2011.606808.
(23) Shaker, M. A.; Elbadawy, H. M.; Shaker, M. A. Improved Solubility, Dissolution, and Oral Bioavailability for Atorvastatin-Pluronic® Solid Dispersions. *Int. J. Pharm.* **2020**, *574*, 118891. https://doi.org/10.1016/j.ijpharm.2019.118891.
(24) Riikonen, J.; Xu, W.; Lehto, V. P. Mesoporous Systems for Poorly Soluble Drugs – Recent Trends. *Int. J. Pharm.* **2018**, *536* (1), 178–186. https://doi.org/10.1016/j.ijpharm.2017.11.054.
(25) Bahl, D.; Bogner, R. H. Amorphization of Indomethacin by Co-Grinding with Neusilin US2: Amorphization Kinetics, Physical Stability and Mechanism. *Pharm. Res.* **2006**, *23* (10), 2317–2325. https://doi.org/10.1007/s11095-006-9062-x.
(26) Müller Reiner H.; David, H.; Nan, J.; Pyo, S. M. SmartPearls – Novel Physically Stable Amorphous Delivery System for Poorly Soluble Dermal Actives. *Int. J. Pharm.* **2018**,

555, 314–321. https://doi.org/https://doi.org/10.1016/j.ijpharm.2018.11.018.
(27) Shen, S.-C.; Ng, W. K.; Chia, L.; Dong, Y.-C.; Tan, R. B. H. Stabilized Amorphous State of Ibuprofen by Co-Spray Drying With Mesoporous SBA-15 to Enhance Dissolution Properties. *Wiley Intersci.* **2009**, *99* (4), 1997–2007. https://doi.org/https://doi.org/10.1002/jps.21967.
(28) Andersson, J.; Rosenholm, J.; Areva, S.; Lindén, M. Influences of Material Characteristics on Ibuprofen Drug Loading and Release Profiles from Ordered Micro- and Mesoporous Silica Matrices. *Chem. Mater.* **2004**, *16* (21), 4160–4167. https://doi.org/10.1021/cm0401490.
(29) Knapik-Kowalczuk, J.; Kramarczyk, D.; Chmiel, K.; Romanova, J.; Kawakami, K.; Paluch, M. Importance of Mesoporous Silica Particle Size in the Stabilization of Amorphous Pharmaceuticals—the Case of Simvastatin. *Pharmaceutics* **2020**, *12* (4), 21–25. https://doi.org/10.3390/pharmaceutics12040384.
(30) Knapik, J.; Wojnarowska, Z.; Grzybowska, K.; Jurkiewicz, K.; Stankiewicz, A.; Paluch, M. Stabilization of the Amorphous Ezetimibe Drug by Confining Its Dimension. *Mol. Pharm.* **2016**, *13* (4), 1308–1316. https://doi.org/10.1021/acs.molpharmaceut.5b00903.
(31) Godec, A.; Maver, U.; Bele, M.; Planinšek, O.; Srčič, S.; Gaberšček, M.; Jamnik, J. Vitrification from Solution in Restricted Space: Formation and Stabilization of Amorphous Nifedipine in a Nanoporous Silica Xerogel Carrier. *Int. J. Pharm.* **2007**, *343* (1–2), 131–140. https://doi.org/10.1016/j.ijpharm.2007.05.022.
(32) Croissant, J. G.; Fatieiev, Y.; Khashab, N. M. Degradability and Clearance of Silicon, Organosilica, Silsesquioxane, Silica Mixed Oxide, and Mesoporous Silica Nanoparticles. *Adv. Mater.* **2017**, *29* (9). https://doi.org/10.1002/adma.201604634.
(33) Croissant, J. G.; Fatieiev, Y.; Almalik, A.; Khashab, N. M. Mesoporous Silica and Organosilica Nanoparticles: Physical Chemistry, Biosafety, Delivery Strategies, and Biomedical Applications. *Adv. Healthc. Mater.* **2018**, *7* (4), 1–75. https://doi.org/10.1002/adhm.201700831.
(34) Rengarajan, G. T.; Enke, D.; Steinhart, M.; Beiner, M. Stabilization of the Amorphous State of Pharmaceuticals in Nanopores. *J. Mater. Chem.* **2008**, *18* (22), 2537–2539. https://doi.org/10.1039/b804266g.
(35) Genina, N.; Hadi, B.; Löbmann, K. Hot Melt Extrusion as Solvent-Free Technique for a Continuous Manufacturing of Drug-Loaded Mesoporous Silica. *J. Pharm. Sci.* **2018**, *107* (1), 149–155. https://doi.org/10.1016/j.xphs.2017.05.039.
(36) Grzybowska, K.; Paluch, M.; Grzybowski, A.; Wojnarowska, Z.; Hawelek, L.; Kolodziejczyk, K.; Ngai, K. L. Molecular Dynamics and Physical Stability of Amorphous Anti-Inflammatory Drug: Celecoxib. *J. Phys. Chem. B* **2010**, *114* (40), 12792–12801. https://doi.org/10.1021/jp1040212.
(37) Dantuluri, A. K. R.; Amin, A.; Puri, V.; Bansal, A. K. Role of α-Relaxation on Crystallization of Amorphous Celecoxib above Tg Probed by Dielectric Spectroscopy. *Mol. Pharm.* **2011**, *8* (3), 814–822. https://doi.org/10.1021/mp100411v.
(38) Knopp, M. M.; Tajber, L.; Tian, Y.; Olesen, N. E.; Jones, D. S.; Kozyra, A.; Löbmann, K.; Paluch, K.; Brennan, C. M.; Holm, R.; Healy, A. M.; Andrews, G. P.; Rades, T. Comparative Study of Different Methods for the Prediction of Drug-Polymer Solubility. *Mol. Pharm.* **2015**, *12* (9), 3408–3419. https://doi.org/10.1021/acs.molpharmaceut.5b00423.
(39) Beiner, M.; Rengarajan, G. T.; Pankaj, S.; Enke, D.; Steinhart, M. Manipulating the Crystalline State of Pharmaceuticals by Nanoconfinement. *Nano Lett.* **2007**, *7* (5), 1381–1385. https://doi.org/10.1021/nl0705081.
(40) Jackson, C. L.; McKenna, G. B. Vitrification and Crystallization of Organic Liquids

Confined to Nanoscale Pores. *Chem. Mater.* **1996**, *8* (8), 2128–2137. https://doi.org/10.1021/cm9601188.

(41) Lu, G. W.; Hawley, M.; Smith, M.; Geiger, B. M.; Pfund, W. Characterization of a Novel Polymorphic Form of Celecoxib. *J. Pharm. Sci.* **2006**, *95* (2), 305–317. https://doi.org/10.1002/jps.20522.

(42) Kozyra, A.; Mugheirbi, N. A.; Paluch, K. J.; Garbacz, G.; Tajber, L. Phase Diagrams of Polymer-Dispersed Liquid Crystal Systems of Itraconazole/Component Immiscibility Induced by Molecular Anisotropy. *Mol. Pharm.* **2018**, *15* (11), 5192–5206. https://doi.org/10.1021/acs.molpharmaceut.8b00724.

(43) Saunders, M.; Podluii, K.; Shergill, S.; Buckton, G.; Royall, P. The Potential of High Speed DSC (Hyper-DSC) for the Detection and Quantification of Small Amounts of Amorphous Content in Predominantly Crystalline Samples. *Int. J. Pharm.* **2004**, *274* (1–2), 35–40. https://doi.org/10.1016/j.ijpharm.2004.01.018.

(44) Hempel, N. J.; Brede, K.; Olesen, N. E.; Genina, N.; Knopp, M. M.; Löbmann, K. A Fast and Reliable DSC-Based Method to Determine the Monomolecular Loading Capacity of Drugs with Good Glass-Forming Ability in Mesoporous Silica. *Int. J. Pharm.* **2018**, *544* (1), 153–157. https://doi.org/10.1016/j.ijpharm.2018.04.035.

(45) Grzybowska, K.; Capaccioli, S.; Paluch, M. Recent Developments in the Experimental Investigations of Relaxations in Pharmaceuticals by Dielectric Techniques at Ambient and Elevated Pressure. *Adv. Drug Deliv. Rev.* **2016**, *100*, 158–182. https://doi.org/10.1016/j.addr.2015.12.008.

(46) Havriliak, S.; Negami, S. A Complex Plane Representation of Dielectric and Mechanical Relaxation Processes in Some Polymers. *Polymer (Guildf).* **1967**, *8* (C), 161–210. https://doi.org/10.1016/0032-3861(67)90021-3.

(47) Vogel, H. Das Temperaturabhangigkeitgesetz Der Viskosität von Flüssigkeiten. *J. Phys. Z.* **1921**, *22*, 645–646.

(48) Fulcher, G. S. Analysis of Recent Measurements of the Viscosity of Glasses. *J. Am. Ceram. Soc.* **1925**, *8* (6), 339–355. https://doi.org/10.1111/j.1151-2916.1925.tb16731.x.

(49) Tammann, G.; Hesse, W. Die Abhängigkeit Der Viscosität von Der Temperatur Bie Unterkühlten Flüssigkeiten. *Zeitschrift für Anorg. und Allg. Chemie* **1926**, *156* (1), 245–257. https://doi.org/10.1002/zaac.19261560121.

(50) Stickel, F.; Fischer, E. W.; Richert, R. Dynamics of Glass-Forming Liquids. II. Detailed Comparison of Dielectric Relaxation, de-Conductivity, and Viscosity Data. *J. Chem. Phys.* **1996**, *104* (5), 2043–2055. https://doi.org/10.1063/1.470961.

(51) Wu, X.; Wang, H.; Liu, C.; Zhu, Z. Longer-Scale Segmental Dynamics of Amorphous Poly(Ethylene Oxide)/Poly(Vinyl Acetate) Blends in the Softening Dispersion. *Soft Matter* **2011**, *7* (2), 579–586. https://doi.org/10.1039/c0sm00633e.

(52) Williams, G.; Watts, D. C. Non-Symmetrical Dielectric Relaxation Behaviour Arising from a Simple Empirical Decay Function. *Trans. Faraday Soc.* **1970**, *66* (1), 80–85. https://doi.org/10.1039/TF9706600080.

(53) Shamblin, S. L.; Hancock, B. C.; Dupuis, Y.; Pikal, M. J. Interpretation of Relaxation Time Constants for Amorphous Pharmaceutical Systems. *J. Pharm. Sci.* **2000**, *89* (3), 417–427. https://doi.org/10.1002/(SICI)1520-6017(200003)89:3<417::AID-JPS12>3.0.CO;2-V.

(54) Kolodziejczyk, K.; Paluch, M.; Grzybowska, K.; Grzybowski, A.; Wojnarowska, Z.; Hawelek, L.; Ziolo, J. D. Relaxation Dynamics and Crystallization Study of Sildenafil in the Liquid and Glassy States. *Mol. Pharm.* **2013**, *10* (6), 2270–2282. https://doi.org/10.1021/mp300479r.

(55) Descamps, M. *Disordered Pharmaceutical Materials*; Wiley-VCH Verlag GmbH &

Co. KGaA: Weinheim, Germany, 2016.
(56) Kremer, F.; Schönhals, A. *Local Dielectric Relaxation by Solvation Dynamics. In Broadband Dielectric Spectroscopy.*; Springer-Verlag: Berlin Heidelberg, Germany, 2003.
(57) Tu, W.; Knapik-Kowalczuk, J.; Chmiel, K.; Paluch, M. Glass Transition Dynamics and Physical Stability of Amorphous Griseofulvin in Binary Mixtures with Low- Tg Excipients. *Mol. Pharm.* **2019**, *16* (8), 3626–3635. https://doi.org/10.1021/acs.molpharmaceut.9b00476.
(58) Chmiel, K.; Knapik-Kowalczuk, J.; Jurkiewicz, K.; Sawicki, W.; Jachowicz, R.; Paluch, M. A New Method to Identify Physically Stable Concentration of Amorphous Solid Dispersions (I): Case of Flutamide + Kollidon VA64. *Mol. Pharm.* **2017**, *14* (10), 3370–3380. https://doi.org/10.1021/acs.molpharmaceut.7b00382.
(59) Chmiel, K.; Knapik-Kowalczuk, J.; Paluch, M. How Does the High Pressure Affects the Solubility of the Drug within the Polymer Matrix in Solid Dispersion Systems. *Eur. J. Pharm. Biopharm.* **2019**, *143* (April), 8–17. https://doi.org/10.1016/j.ejpb.2019.08.003.
(60) Chmiel, K.; Knapik-Kowalczuk, J.; Jachowicz, R.; Paluch, M. Broadband Dielectric Spectroscopy as an Experimental Alternative to Calorimetric Determination of the Solubility of Drugs into Polymer Matrix: Case of Flutamide and Various Polymeric Matrixes. *Eur. J. Pharm. Biopharm.* **2019**, *136* (July 2018), 231–239. https://doi.org/10.1016/j.ejpb.2019.01.025.
(61) Ignaczak, W.; Skov, A. L.; El Fray, M. Interfacial Polarization in Thermoplastic Basalt Fiber-Reinforced Composites. *Polymers (Basel).* **2020**, *12* (7), 1–16. https://doi.org/10.3390/polym12071486.
(62) Baeza, G. P.; Oberdisse, J.; Alegria, A.; Couty, M.; Genix, A. C. A High-Temperature Dielectric Process as a Probe of Large-Scale Silica Filler Structure in Simplified Industrial Nanocomposites. *Phys. Chem. Chem. Phys.* **2015**, *17* (3), 1660–1666. https://doi.org/10.1039/c4cp04597a.
(63) Gitsas, A.; Floudas, G.; Wegner, G. Effects of Temperature and Pressure on the Stability and Mobility of Phases in Rigid Rod Poly [Formula Presented]-Phenylenes). *Phys. Rev. E - Stat. Physics, Plasmas, Fluids, Relat. Interdiscip. Top.* **2004**, *69* (4), 8. https://doi.org/10.1103/PhysRevE.69.041802.